Flexible implementation of modulated localization microscopy based on DMD

Abigail Illand, Pierre Jouchet, Emmanuel Fort, Sandrine Lévêque-Fort

Flexible implementation of modulated localization microscopy based on DMD

Abigail Illand[1], Pierre Jouchet[1*], Emmanuel Fort[2] and Sandrine Lévêque-Fort[1]

1- Institut des Sciences Moléculaires d'Orsay, Université Paris Saclay, CNRS UMR8214, 91405 Orsay
2- Institut Langevin, ESPCI Paris, Université PSL, CNRS, 75005 Paris

(*) current address : Moerner Lab, Chemistry department, Stanford University, US.

Initial Submission on 03/12/2023

Abstract : Localization microscopy of individual molecules allows one to bypass the diffraction limit, revealing cellular organization on a nanometric scale. This method, which relies on spatial analysis of the signal emitted by molecules, is often limited to the observation of biological objects at shallow depths, or with very few aberrations. The introduction of a temporal parameter into the localization process through a time modulated excitation was recently proposed to address these limitations. This method called ModLoc, is demonstrated here with an alternative flexible strategy. In this implementation, to encode the time modulated excitation a digital micromirror device is used in combination with a fast demodulation approach, and provides a two-fold enhancement in localization precision.

Keywords :single molecule localization, structured excitation, fluorescence, microscopy, DMD

1- Introduction

Single Molecule Localization Microscopy (SMLM) is revolutionizing biology by revealing structural information with a resolution far below the diffraction limit, offering observation down to few nanometers as opposed to several hundred nanometers in conventional optical imaging methods[1–4]. This fluorescence imaging approach is based on the detection and localization of individual molecules within the focal volume of the microscope, emitting signals randomly over time (see Fig. 1-a). The transverse position (x, y) of the fluorescent emitter can thus be extracted by a spatial analysis of its PSF typically based on a Gaussian model for computational simplicity. Recently more complex models, in particular with the introduction of experimental PSF values have been proposed (see Fig. 1-b). This position is obtained with an accuracy and precision well below the diffraction limit, depending primarily on the number of emitted photons (N) $\sigma_{x,y} \sim \sigma_{PSF}/\sqrt{N}$, and also on the size of the PSF[5]. The principle of localization, enabling the tracking of individual molecules, emerged in the 1980s. However, it had to wait for the development of new photophysical strategies to be applied to the observation of biological structures labeled with many fluorescent molecules, which must be prevented from emitting simultaneously but randomly, thus permitting their individual localization. The fluorescent molecules in the sample operate in a regime known as blinking, achievable through various modalities such as PALM (Photo-Activated Localization Microscopy)[1,2,6], where photophysical control is applied to photoactivatable or photoconvertible fluorescent proteins; (d)-STORM (for (direct)-Stochastic Optical Reconstruction Microscopy)[3,7], where organic fluorophores capable of emitting numerous photons can be compelled to transition into energy states enabling separate observation; or more recently, (DNA)-PAINT (for Points Accumulation for Imaging in Nanoscale Topography), where the brief pairing of DNA strands marked with a fluorescent probe also induced a sparsity of observed fluorescent emitters[8]. Thus, in each acquired image, only a subpopulation of individual molecules is detected and localized, typically requiring the acquisition of between 5,000 to 80,000 images to explore the entire structure and reconstruct the final super-resolved image (see Fig. 1 a-b).

This localization process provides only transverse spatial information (x, y) and complementary strategies must be implemented to retrieve the axial position along the optical axis (z)[9]. The methods primarily used involve shaping the PSF to break its axial symmetry, such as adding a cylindrical lens to introduce controlled astigmatism[10] (see Fig. 1-c). Other families of PSF shaping have been developed to enhance performance in terms of both observation depth and axial precision, which tends to vary within the observation volume[9]. Utilizing the intrinsic properties of fluorescence emission, such as supercritical emission[11–13], can also provide axial information with an absolute information on the elevation of the emitters regarding the interface

coverslip/sample, but is limited in observation depth to 500-600 nm[14]. Using fluorescence emission interferences obtained through double objective configuration (4π) permits to achieve a resolution of a few nanometers but proves complex to implement[15,16]. Alternatively, it has been shown that the introduction of a diffraction grating permits to take advantage of fluorescence self-interference[17], enabling deep imaging but requiring high sampling of the spatially structured PSFs.

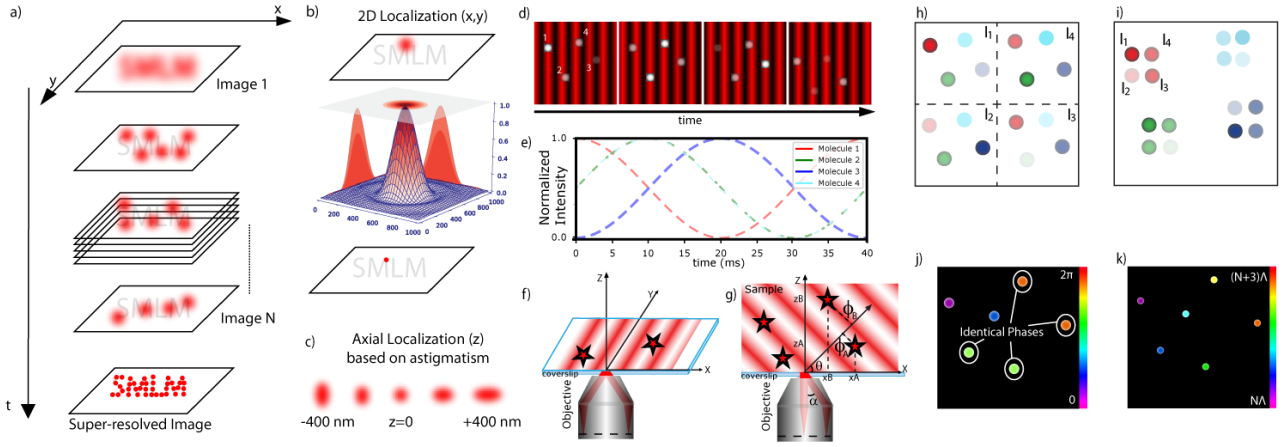

Fig1: (a-c) Principle of the single molecule localization microscopy. a) Only part of the molecules emitted at each image resulting in the observation of a super-resolved image when successive images of the same region are acquired. b) For each image acquired, the position of the molecules on this image are obtained from fitting a 2D gaussian function. c) The axial position of the molecule compared to the focus plane can then be obtained by introducing an astigmatic aberration. (d-f) Principle of the single molecule localization using time-varying signal. d) A structured illumination is shifted temporally. e) The signal emitted by the fluorophores will result in a sinusoid and the phase depends on the position of the fluorophore in the field of view. f-g) The structured illumination can be along the (x,y) plane or along the (x,z) plane depending on the position of the two beams in the back focal plane. h) The signal can be demodulated in a single camera frame. Each image corresponding to one position of the excitation is sent to 4 separated parts of the camera. The 4 fluorophores can be localized utilizing their respective intensities in each part of the camera. i) The signal can alternatively be demodulated in a single camera frame and each fluorophore will have four images around its original position. j) The demodulated signal gives wrap information on the phase of the fluorophore. k) Signal can be unwrapped using the position of the molecule.

During the localization process, both transverse and axial, any deformation of the PSF induced, for example, by simple defocus or more complex aberrations related to the sample, affects the localization precision. Analyzing the PSF based solely on spatial parameters impacts both 2D and 3D localization as well as the ability to observe samples in depth.

We have thus proposed the incorporation of a temporal parameter to extract localization information with enhanced and uniform precision in the observation depth[18]. Specifically, we drew inspiration from a method utilizing spatial properties of illumination to track the scattering signal of a polystyrene bead within a structured excitation pattern. Created by temporally displaced interferences on the sample[19], these travelling wave interference induces a modulated scattering, with the phase reflecting the molecule's position. The TWT (Traveling Wave tracking) allows one to position along two directions with a lateral resolution of 3 Å and with a time resolution in the microsecond range, and was in particular applied to reveal myosin step displacement[20]. As this setup was designed for observing a single object in the field of view demodulation could be performed with a photodiode and synchronous detection to extract the phase of the modulated signal from the sole object present and derive its position evolution within the field of view. We have recently revisited this concept to adapt it for wide field localization of single fluorescent molecules, necessitating the development of synchronous detection compatible with a camera. This adaptation involves handling a limited number of fluorescence photons associated with emission events that occur stochastically during acquisition. This novel microscopy approach, subsequently named ModLoc[21,22] (Modulated Localization), permits the extraction of molecule positions over a wide field (typically 50 µm x 50 µm) with a localization precision increased by a factor up to 2.4 in the direction of the modulation, either lateral or axial, and with a unique uniform precision along the axial direction[21]. This method is also undergoing various developments within different research teams, featuring diverse implementations aimed at enhancing lateral or axial resolution. These variations go by names such as Simple[23], Simflux[24], or Rose[25,26], each distinguished by its strategy for excitation and/or detection of the modulated fluorescence signal. It is worth noting that these methods differ from the Minflux[27] approach, which proposes a series of sequential measurements

dedicated to each emitter for different positions of the structured excitation beam, at the cost of a reduced field of view[28]. However, this enables achieving sub-nanometer resolution individually for each event[29–31]. In the wide-field approaches, the resolution improvement is uniform for all molecules, as it is achieved through phase measurement of the modulation, relying on an identical displacement of the structured illumination for all emitters.

In a conventional SMLM microscope, this necessitates replacing the uniform excitation of the sample with a sinusoidal excitation pattern displaced in the desired direction for improvement (see. Fig. 1-d). For instance, if the illumination is applied along the transverse direction x with a temporal modulation frequency Ω and a spatial pitch Λ, it can be expressed in the form:

$$\boldsymbol{I(x,t) = I_0\left(1 + m\cos\left(\frac{2\pi}{\Lambda}x + \Omega t\right)\right)} \qquad (1)$$

With I_0 is the average light intensity over the entire field and m is the contrast of the illumination pattern. In the regime of linear excitation (outside of saturation), the fluorescence signal from a molecule is proportional to the light intensity it receives. The photon flux $N(x,t)$ detected from a fluorescent emitter illuminated by the excitation field described by equation (1), positioned at location x, is given by:

$$N(x,t) = N_0(1 + m\cos(\Phi(x) + \Omega t)) \qquad (2)$$

With the phase $\Phi(x) = \frac{2\pi}{\Lambda}x$ and N_0 the mean photons flux detected and associated to I_0. As can be seen in Figure 2-e, the temporally modulated signals of different fluorescent molecules carry information about the molecule's position in its phase Φ(x). Modulated excitation can thus be applied to any direction, either along x or y, and for the z direction a tilted version along xz can be proposed (see Figure 2-f).

Among the various developments, one key difference lies in the strategy to demodulate the signal and extract the position associated with the phase. The simplest approach involves sequentially acquiring 3 or 4 images corresponding to each position of the structured illumination. However, to mitigate biases related to molecules transitioning between a bright state (ON) and a dark state (OFF), typically, 2 additional images are acquired, framing the images necessary for demodulation. Depending on the camera used and the chosen field of view, this can lead to the exclusion of events from single molecules whose ON state is too short compared to the time required for this sequential acquisition. For instance, with an sCMOS camera operating at 400 Hz, it is estimated that around 30% of molecules are not considered[32] (for an average ON time of 15 ms). We have developed a different approach where the 4 intensity values necessary for demodulation are acquired within the same camera frame, either in 4 distinct sub-regions of the camera[21] (see fig. 1-h) or to form a compact pattern creating a composite PSF[22] (see Fig. 1-i). This enables demodulation at a frequency around the kHz range, significantly higher than the acquisition frequency of cameras, thereby capturing the entirety of events.

Since the illumination structure is periodic, it is apparent that molecules at different positions in the field exhibit distinct phases (see. Fig. 1-j). However, certain molecules (2 and 4) may share identical phases. To derive the final position within the observation field, a Gaussian fitting analysis is applied to each molecule of the image, determining the fringe containing the molecule[22]. This information is then coupled with phase data that precisely locates the molecule within the identified fringe (see. Fig. 2-k). The Cramer Rao Lower Bounds (CRLB), outlining the theoretical precision of localization achievable for this method under 4-point demodulation, no background noise, and maximum excitation contrast, adopt a straightforward form:

$$\Delta_x = \frac{\sigma_{PSF}}{\sqrt{N\left(1 + \frac{4\pi^2\sigma_{PSF}^2}{\Lambda^2}\right)}} \qquad (3)$$

where we notably find the pitch of the excitation pattern, and the localization precision improves by reducing the spatial period.

In this article, we introduce a novel combination of active optical elements commonly employed in structured illumination microscopy (SIM)[33–39]. This potentially enhances the synergy of these two approaches, providing information at different scales. By using digital micromirrors device (DMD) composed of a matrix of orientable micrometric mirrors [39–44], it provides a greater flexibility in the fringe spacing of excitation or orientation. The use of a DMD, previously proposed in a sequential approach[23], is presented here in combination with demodulation using galvanometric mirrors. This setup is designed to create the four sub-regions within the same camera frame, eliminating constraints on the emission duration of the molecules.

2- Materials and Methods

2.1 Optical implementation of the ModLoc setup

The ModLoc microscope is developed around an inverted Nikon TiE microscope body with a x60 1.49 NA objective (see fig. 2-a), with a 500 mW 640 nm laser (LPX-640, Oxxius), and a filter set from Semrock (Di02-R635-25x36 , BLP01-635R-25) .

The figure 2 represents various configurations for the excitation and detection implemented by our team (see Fig.2 b,d,e) , and in particular the current one based on the DMD and galvanometric mirrors (see fig.2 c and f). Previously, the sinusoidal excitation was generated by directly interfering two beams in the biological sample. The introduction of an electro-optic modulator then permits the displacement of interferences on the sample, typically at 1.2 kHz, to retrieve the 4 needed intensity values (see fig. 2-b). This implementation limits the flexibility in terms of pitch pattern size and orientation. The introduction of DMD (Vialux, DLP discovery 4100) mitigates these last two points while raising the issue of preserve illumination power (described in details below). The laser beam was expanded to cover the entire surface of the micro-mirror array. The plane of the DMD was then projected onto the sample plane through two consecutive lens relays. The first relay is an afocal system that facilitates access to the Fourier plane where the diffraction orders become visible. Consequently, a diaphragm and a beam blocker can be placed in this plane to isolate only the ±1 orders. The second relay, comprising the tube lens and the objective lens, was employed to recombine the two selected beams on the sample (see Fig. 2-c).

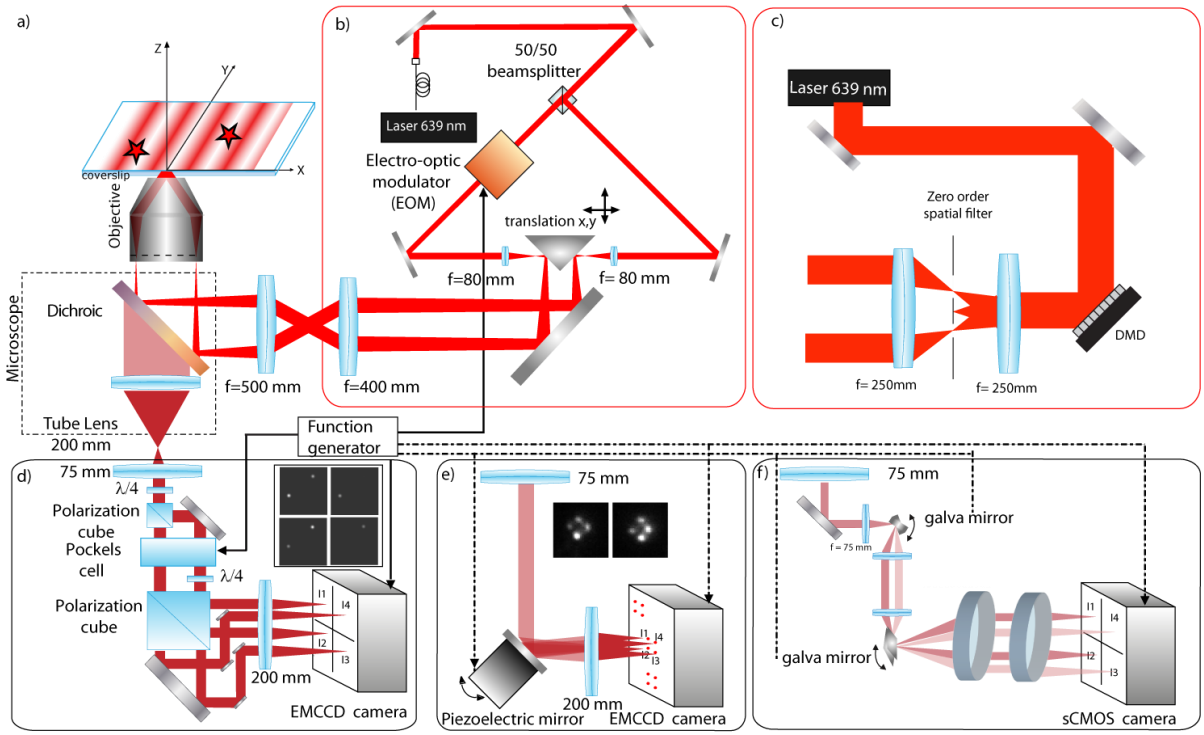

Fig. 2 : Experimental setup with the different modalities to modulate and demodulate the fluorescence signal. a) Microscope parts where the tube lens, dichroic and objective are. On the sample fringes are created along the x axis. b) This modulation can be generated with interferences of a laser beam divided into two equal paths. An EOM on one of the arms introduces the time variation of the signal that the fluorophores will receive. c) The modulation can be generated using a DMD. The time variation of the signal is then introduced by shifting the active mirrors on the DMD. Once the modulation of the signal of fluorescence is created, it must be demodulated in the detection. Three solutions are possible using an active element that can either be a Pockels cell, a mirror mounted on a piezo or two galvanometer mirrors. These actives elements are synchronized with the position of the fringes on the sample.

The fluorescence image is detected either directly with a sCMOS camera (Hamamatsu, orca flash 4 v2) for some calibrations steps which only requests intensity measurements, but for the detection of the phase of the modulated fluorescence, a home-made demodulation module needs to be used in front of the camera (see fig 2d-f). As represented in fig. 2.d-f the common goal of these demodulation modules is to address the four different localization events corresponding to the 4 positions of the structured illumination in four different locations of the camera at a frequency close to kHz, and thus averaging over at least 20 to 60 cycles of modulation during the integration of the full camera frame typically acquired at 20 to 50 Hz. The use of a Pockels cell permits to rely on a highly stable optical module, as no moving element is used, but limits in terms of field of view and demodulation efficiency[21]. In contrary using active mirrors can mitigate these last two points, while the configuration based on piezo-electric mirror (S 330.2 SL, Physik Instrument) tends to be slow and the generated PSF could impact the observed density[22]. The galvanometric mirrors employed here (Scannermax, Saturn 1b) thus appear as a good compromise in terms of speed, field of view and demodulation efficiency, since they can fully address the intensity acquired in a subarray of the image for a given configuration of the DMD at up to 600 Hz . The first galvanometric mirror is placed in the image plane and conjugated with the second one, which permits to create the four subarrays on the camera.

2.2 Operation of a Digital micro-mirror array (DMD)

A DMD consists of an array of micro-mirrors, each with two active positions: an "ON" position where the mirror is oriented at an angle of +12°, and an "OFF" position where the mirror is oriented at -12°. All mirrors can be independently oriented in one of these two directions to create the desired image on the array. While DMDs are commonly used in video projectors, they have also found extensive applications in creating structured illumination for sectioning[45,46] or achieving a twofold resolution enhancement in Structured Illumination Microscopy (SIM)[40–42,47,48].

Two approaches have been employed in SIM using DMDs. The first method involves the direct projection of the image onto the DMD[46]. This approach necessitates incoherent illumination, such as using an LED, or the introduction of an element like a diffuser to eliminate spatial coherence. The second method employs the DMD as a diffraction grating, where interference is created in the plane of the sample. The latter method requires coherent illumination, such as a laser[48], and will be employed subsequently to create a diffraction grating on the sample.

Initially, the DMD functions as an echelle grating, with the mirrors forming a sawtooth diffraction grating. When all the mirrors are oriented in the same direction, multiple diffraction orders are present. The first diffraction grating is thus created when all the mirrors share the same orientation. The angle at which the laser strikes the DMD determines the distribution of light intensity in the different orders. This angle, known as the blaze angle in the case of an echelle grating, can be optimized at the wavelength used to maximize the light power in the first diffraction order of the grating[47]. Figure 3-a illustrates the diffraction grating formed when all the mirrors are at the same angle, and the blaze angle is not optimized. The light intensity is evenly distributed among four main orders. When the angle is well chosen (Figure 3-b), it is possible to concentrate the maximum intensity in a single order. However, some light will inevitably be lost in the other diffraction orders. This light loss is a drawback when using DMD for applications requiring high laser power. This initial diffraction grating creates the signal envelope.

Secondly, once a pattern is applied to the DMD, a second diffraction grating is created in each order. This grating contains the information needed to create fringes on the sample. If a vertical alternation between mirrors in the "ON" position and mirrors in the "OFF" position is applied, the diffraction orders obtained are shown in Figure 3-c. In Figure 3-c, nine sub-networks are visible, each containing fringe information. In the center, there is a main grating where the majority of the light power is concentrated. There are four less intense secondary gratings and finally, four others which are lower but still visible. There are numerous other sub-arrays that are less and less intense and therefore not visible in the figure.

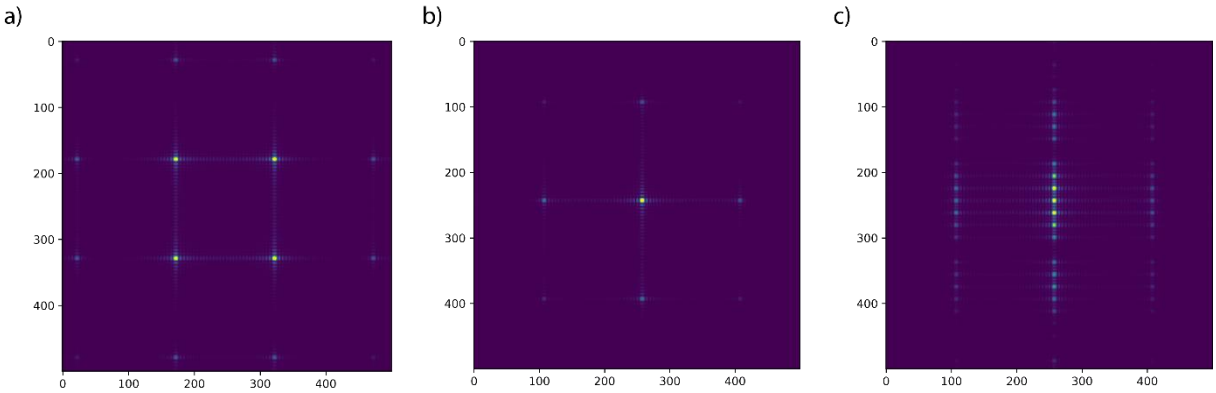

Fig. 3 Simulations of the resulting patterns in the Fourier plane after the DMD depending on the angle between the beam and the DMD and on the pattern applied to the mirrors. a) If all mirrors are displaying the same orientation (ON), the resulting pattern can either be a) or b). In the case of a) the blaze angle is not optimized resulting in an equal repartition of the light intensity in four different points. When the blaze angle is optimized most of the light can be sent to only one point in the center. The resulting diffraction pattern will be the desired one and is displayed in b). c) Diffraction pattern when the blaze angle is optimized, and the mirrors position are alternating between ON and OFF position horizontally. Each previous points of the pattern in b) will now form a new pattern. Each pattern corresponds to the Fourier transform of a squared signal and the central one is concentrating the most intensity.

To generate the fringes on the sample, we are interested in orders 0 and ±1, with the angle between the orders denoted as θ. It should be noted that retaining a maximum of around 13% of the incident light is possible when only these three orders are considered[49]. The complex amplitude of the different orders is then determined by $A_{+1} = Ae^{i\delta}$, $A_{-1} = Ae^{-i\delta}$ and $A_0 = \varepsilon Ae^{i0}$. A is the amplitude, ϵ is the ratio between the amplitude of order 0 and the amplitude of orders ±1 and δ is the phase factor between orders 0 and +1.

$$\delta = k\Delta + \phi$$

With Δ is the optical path difference between the two orders with $\Delta \sim x \sin(\theta)$ with x behing the pattern direction, ϕ is an arbitrary spatial phase and k is the wave number : $k = 2\pi/\lambda$

If the 0 order is filtered, two coherent beams will be superimposed. The resulting intensity follows the following formula:

$$I = \left|A_{+1} + A_{\_1}\right|^2 = 4\,A^2 cos^2\delta = 2A^2(cos2\delta + 1)$$

The inter-fringe distance can be written $\Lambda_{sample} = \lambda/(2sin\theta)$. The angle θ depends on the pattern applied to the DMD whose inter-fringe distance can be called Λ_{DMD} and the total magnification of the system M. These quantities are linked by the formula $sin\theta = M * \lambda\ /\Lambda_{DMD}$.

It is feasible to independently control the position of all DMD mirrors, enabling the creation of lines or arrays. To modulate the intensity of fluorophores and determine their position based on the phase of their modulated emission, it is essential to have four intensity points. A DMD simplifies achieving this fringe shift by shifting the period of one mirror each time, as illustrated in Figure 4.

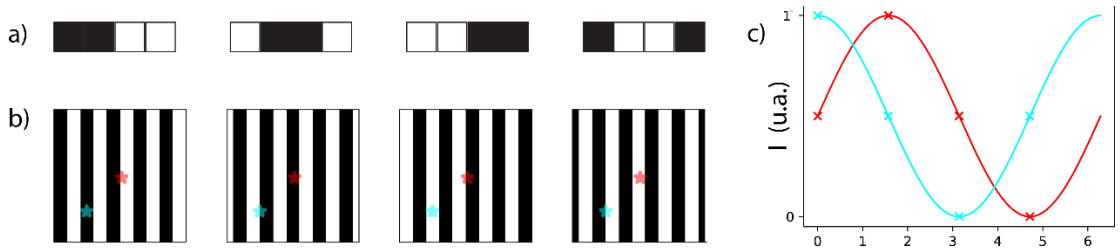

Fig. 4: Creation of the modulation with the DMD. a) Schematic representation of one period of the DMD at four different time scales. Black squares correspond to mirrors in the OFF position and white squares mirrors in the ON position. To modulate the signal the mirrors are shifted by one quarter of the period each time which corresponds to one mirror. b) Schematic representation of the fringes on the sample with two static fluorophores (stars red and blue) in the field of view. Each shift to the mirrors in a) corresponds to a movement of the fringes. c) The resulting fluorescence emitted by the two fluorophores is 2 sinusoids with the same period but a different phase.

If we consider two fluorophores located at different positions on the sample (Figure 4-b), the resulting modulation will exhibit different phases depending on the fluorophore (Figure 4-c). Consequently, configuring the DMD requires providing an inter-fringe distance on the DMD of a multiple of 4, with at least 4 mirrors per period (Figure 4-a); otherwise, it is impossible to obtain the four intensity points required for demodulation. To achieve the best precision in localizing the fluorophore, it is essential to have the smallest possible inter-fringe distance on the sample. However, the minimum size achievable is constrained by diffraction, meaning fringes on the sample cannot be smaller than 240 nm. The system's magnification must be chosen to obtain small-sized fringes while staying within this diffraction limit and ensuring a multiple of 4 mirrors per period on the DMD. With the chosen lenses and the pitch of our DMD set at 10.8 µm, it is possible to have an inter-fringe distance of 288 nm with 8 mirrors used per period on the DMD (4 "ON" and 4 "OFF").

Results

3.1 Verification of the experimental parameters of the structuration excitation based on DMD

By employing modulated excitation, the precision of localization no longer depends solely on the number of photons and the background signal but also on the parameters of the fringe pattern. Among these parameters, the spatial period and modulation contrast play crucial roles. To enhance localization precision, it is ideal to have the smallest possible spatial period, i.e., 240 nm, and the highest modulation contrast, i.e., 1. Initially, it is necessary to experimentally determine the parameters of the fringe pattern to ensure their proximity to the ideal values. Subsequently, these determined parameters are utilized to calculate the positions of the molecules.

To measure the modulation contrast, a sample of isolated fluorescent beads with a diameter of 40 nm was utilized. A camera was directly employed to image the sample (without any demodulation element) and was synchronized with the position of the mirrors on the DMD. For each position of the mirrors on the DMD, an image with an acquisition time of 20 ms was captured by the camera before moving on to the next position on the DMD and acquiring another image on the camera. This method enables the plotting of the temporal intensity variation for different beads in the sample, as depicted in the figure. Subsequently, the modulation contrast can be calculated using the formula $m = \frac{I_{\max} - I_{min}}{I_{\max} + I_{min}}$. An average value of 0.8 is then obtained for the modulation contrast in our experiment. While this contrast may not be perfect, it could be influenced by the size of the fluorescent beads (40 nm in diameter) and the sub-sampling of the period with only four points. In the subsequent steps, we will use this value of 0.8 for determining the positions of the molecules and compare it to the theoretical expectations.

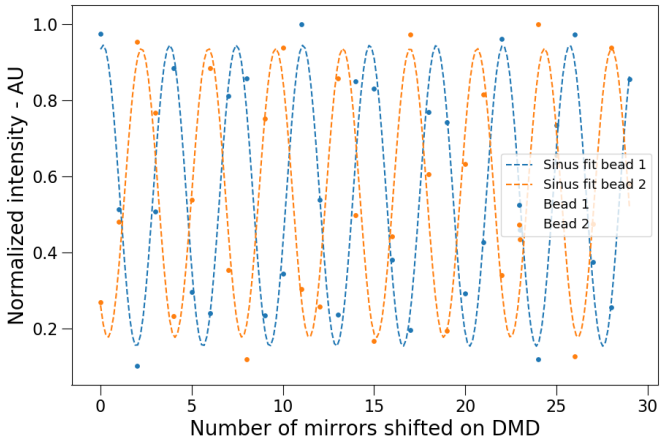

Fig. 5: Experimental intensity data from two 40 nm nanobeads in the field of view where the fringes were shifted using the DMD as described in fig.4. For each shift of the mirrors on the DMD, one frame was acquired on the camera.

To measure the size of the fringes, given the absence of a nanometric stage in this microscope, it was not feasible to move the sample in small steps to determine the spatial period of the illumination. An alternative approach was employed, utilizing a sample of fluorescent beads at a much higher concentration to achieve an almost uniform sample. By observing this dense sample, the fringes can be directly viewed on the camera. For a chosen period of 8 mirrors on the DMD, an experimental inter-fringe distance of 302 nm was measured.

By applying these experimental parameters to the Cramér-Rao equation, it becomes possible to determine the theoretical localization precision of our experiment. This calculation had previously been conducted using an excitation interferometer[22], and the results are comparable when using a DMD. Figure 6 illustrates the performance we can anticipate with the DMD, in particular depending on the spatial frequency of the pattern and contrast values. As expected the optimal gain corresponds to the smallest pitch pattern applicable on the sample limited by the NA of the objective (see Fig 6-a). However, an improvement in localization precision compared to a conventional approach using Gaussian fitting can be observed for several contrast/pattern pairs, which still leaves some flexibility to the method. The expected localization precision depending on the number of photons is represented in fig. 6-b) for various background values, and an improvement factor of at least 2 is expected.

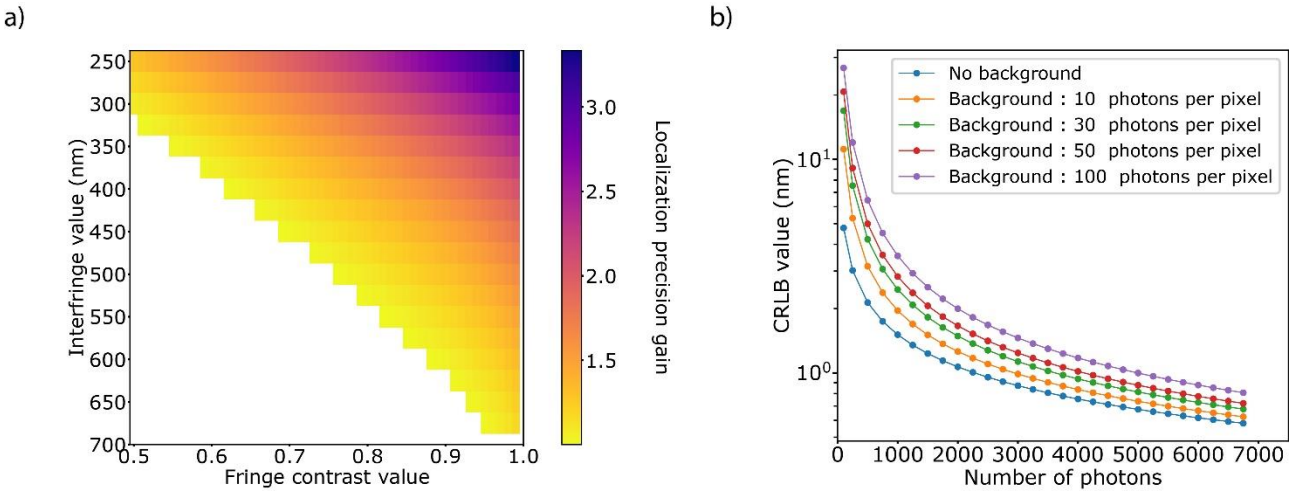

Fig. 6: a) Expected gain for the localization precision depending on the spatial frequency of the pattern and of the pattern contrast compared to conventional gaussian approach. Only localization precision gain higher than 1.1 are represented. Number of photons emitted = 2000, background = 10 photons per pixels b) Expected precision (CRLB) for the various value of background as a function of the number of photons for a maximum contrast and an inter-fringe distance of 300 nm.

3.2 Experimental validation on fluorescent nanobeads.

To validate the use of DMD-based excitation, a lateral precision analysis was conducted on controlled samples. Isolated fluorescent beads with a diameter of 40 nm and an emission wavelength centered at 680 nm were employed. This type of sample necessitates low laser power to approach the number of photons emitted by a single molecule closely. Additionally, it permits to measure the position of each bead repeatedly over several successive acquisitions without observing photobleaching.

A comparison between the bead position found by the Gaussian fitting method and the position determined using demodulation of the fluorescence signal was performed. For demodulation signal processing, detection with galvanometric mirrors was set up upstream of the camera. The frequency of the mirrors was chosen to be 100 Hz, a relatively low value to avoid being affected by the rise time of the galvanometers. Unlike dSTORM single-molecule emissions, which can have a short emission time and may fade out during a camera image, the beads exhibit long and stable emission times. This characteristic enables optimal localization precision even with a few modulation/demodulation cycles during an image.

The classic position of the beads is the average of the four positions obtained for the same bead in the four quadrants. In contrast, the ModLoc position takes advantage of the phase of the signal according to the direction in which the modulation has been applied. For each bead in an acquisition, there is a series of positions obtained by Gaussian fitting and a series of positions obtained by the ModLoc method. The standard deviations of each series correspond to the respective localization precision of each method.

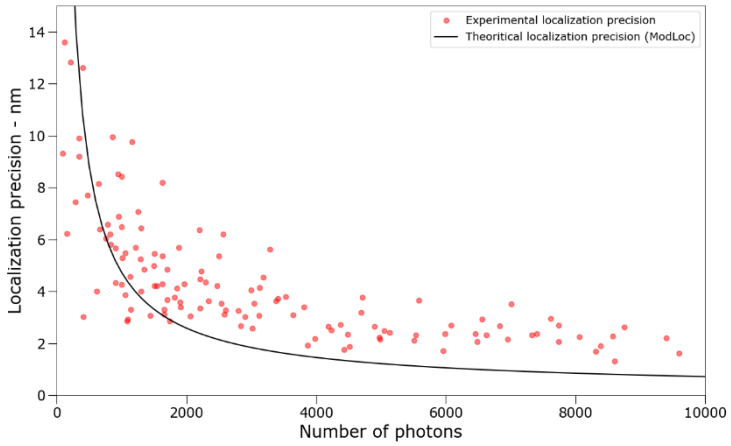

Fig. 7: Experimental localization precision of ModLoc in comparison with the Cramer-Rao Lower bound theory. The localization precision as a function of the number of photons comes from isolated 40 nm nanobeads emitting in red.

The figure depicted in Fig. 7 represents the ModLoc localization precision for various nanobeads as a function of the number of photons. In a series of acquisitions, the localization precision of different nanobeads is plotted against the number of photons it emits. Since not all beads emit the same number of photons, this measurement provides the corresponding precision experimentally obtained as a function of the number of photons emitted. These experimental results align well with the theoretical localization precision calculated by Cramér-Rao lower bound (represented in black in Fig. 7) with a modulation contrast of 0.8 and a fringe period of 310 nm generated by the DMD illumination.

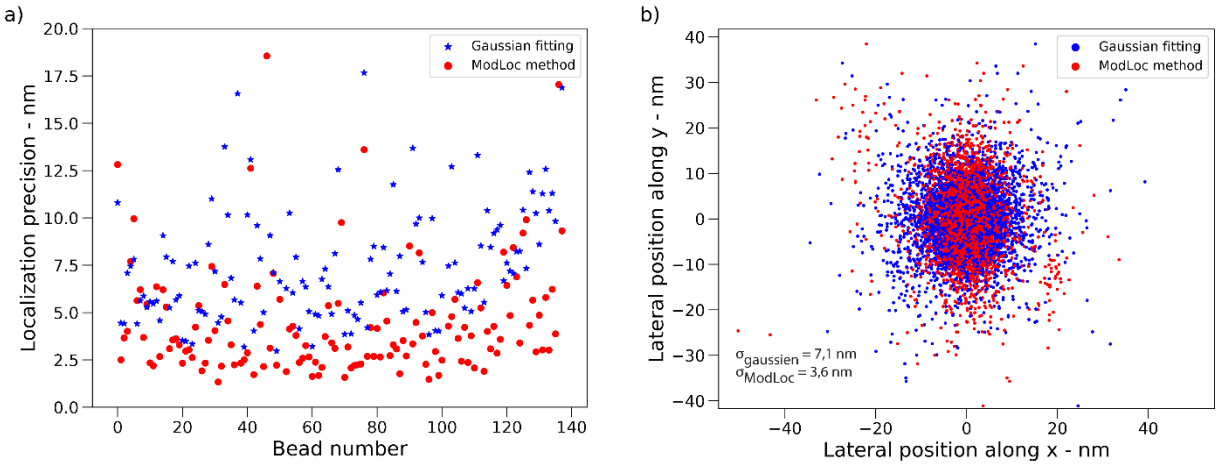

Fig 8 : The comparison of experimental localization precision obtained on beads is presented as follows: (a) Comparison of localization precision obtained using ModLoc (red dots) and Gaussian method (blue stars). (b) Reconstruction of the positions obtained by Gaussian fitting and by ModLoc, centered around the mean positions for each bead, resulting in an improvement factor of 2 for localization precision using the ModLoc method.

A second analysis involves comparing the localization precision depending on the method chosen to localize the bead. Figure 8-a illustrates the precision obtained over a series of acquisitions for several beads using modulation to find their position (red dots) or using a Gaussian fitting (blue dots), clearly highlighting the improvement. Figure 8-b presents the same data but in a different representation: the set of successive localizations of all the beads is depicted as a cloud of points where each localization is centered around the average position of the bead. The red points represent the ModLoc localization, while the blue points are obtained by Gaussian fitting. An improvement in precision along the applied modulated direction (x) is visible, where the red points are more clustered in this direction than along the y direction, where no modulation has been applied. The median for all beads using a Gaussian fit gives an average localization precision of 7.1 nm, compared with an average of 3.6 nm when using ModLoc to position the beads. Therefore, there is a factor of 2 improvement, consistent with theoretical predictions.

3- Discussion and conclusion

This work research presents an alternative implementation of structured excitation for enhanced localization microscopy, integrating the DMD-based excitation with a simultaneous demodulation approach within a single camera frame based on galvanometric mirrors. This implementation demonstrates a twofold improvement in precision compared to classical Gaussian fitting. We showcase this enhancement across various levels of emitted photon numbers and for the smallest achievable pitch in our current setup, specifically an inter-fringe distance of 300 nm.

This DMD-based implementation, designed to be compatible with the diverse kinetics of single-molecule emission, opens the door to a versatile implementation of ModLoc. The micro-mirrors enable the fine-tuning of spatial parameters of the structured excitation, permitting the adaptation to different objective magnifications and numerical apertures. Moreover, it effortlessly adjusts the commuting frequency up to the kHz regime, permitting to optimize easily the applied modulation depending on the single molecule strategy used, but also paving the way for faster implementation needed for an extension to single-particle tracking.

However, significant challenges arise from the constraints associated with the blaze grating configuration when using coherent excitation. While low output excitation power after the DMD is not problematic for SIM microscopy, as low excitation levels are typically needed to prevent photobleaching, the requirement for multi-wavelength excitation in multicolor imaging demands a specific implementation to maintain efficient wavelength-dependent coupling on the DMD with different lasers[42,44,47]. Conversely, in SMLM, multi-target imaging is now widely achieved with a single laser excitation, but with fluorophores with close spectral emissions (less than 30 nm apart) to enable spectral demixing based on ratiometric measurements[50–53]. Thus, the primary limitation for SMLM lies in the low efficiency of the DMD, where only approximately 13% of the illumination is reflected. For dSTORM experiments, where several kW/cm² are typically required to initiate the single-molecule regime, a 1W laser would limit the field of view to less than 25x25 µm². Hence, lasers of several watts are necessary for dSTORM to preserve a larger field of view which can be a major limitation. This challenge can be mitigated in conjunction with DNA-PAINT imaging, where lower irradiance (typically less than 0.5 kW/cm²) is needed. This lower requirement is compatible with commonly used laser below 1W while still offering a more standard field of view (50x50 µm²).

Given the widespread use of DMDs in SIM microscopy, there is clearly a potential for the convergence of these ModLoc and SIM implementations into a single instrument for 2D or 3D imaging[54], offering an original multiscale microscope.

Acknowledgments :

A.I and P.J. acknowledges a master funding from GDR ImaBio, and P.J a PhD funding from IDEX Paris Saclay (ANR-11-IDEX-0003-02). This work was supported by the AXA research fund, the ANR (LABEX WIFI, ANR-10-LABX-24), ANR MSM-Modulated super-resolution microscopy (ANR-17-CE09-0040), the valorization program of the IDEX Paris Saclay and of Labex PALM (ANR-10-LABX-0039-PALM).

References :

1. Betzig, E., Patterson, G.H., Sougrat, R., Lindwasser, O.W., Olenych, S., Bonifacino, J.S., Davidson, M.W., Lippincott-Schwartz, J., and Hess, H.F. (2006). Imaging Intracellular Fluorescent Proteins at Nanometer Resolution. Science *313*, 1642–1645. 10.1126/science.1127344.

2. Hess, S.T., Girirajan, T.P.K., and Mason, M.D. (2006). Ultra-High Resolution Imaging by Fluorescence Photoactivation Localization Microscopy. Biophysical Journal *91*, 4258–4272. 10.1529/biophysj.106.091116.

3. Rust, M.J., Bates, M., and Zhuang, X. (2006). Sub-diffraction-limit imaging by stochastic optical reconstruction microscopy (STORM). Nat Methods *3*, 793–796. 10.1038/nmeth929.

4. Dickson, R.M., Cubitt, A.B., Tsien, R.Y., and Moerner, W.E. (1997). On/off blinking and switching behaviour of single molecules of green fluorescent protein. Nature *388*, 355–358. 10.1038/41048.

5. Ober, R.J., Ram, S., and Ward, E.S. (2004). Localization Accuracy in Single-Molecule Microscopy. Biophysical Journal *86*, 1185–1200. 10.1016/S0006-3495(04)74193-4.

6. Biteen, J.S., Thompson, M.A., Tselentis, N.K., Bowman, G.R., Shapiro, L., and Moerner, W.E. (2008). Super-resolution imaging in live Caulobacter crescentus cells using photoswitchable EYFP. Nat Methods *5*, 947–949. 10.1038/nmeth.1258.

7. Heilemann, M., van de Linde, S., Schüttpelz, M., Kasper, R., Seefeldt, B., Mukherjee, A., Tinnefeld, P., and Sauer, M. (2008). Subdiffraction-Resolution Fluorescence Imaging with Conventional Fluorescent Probes. Angewandte Chemie International Edition *47*, 6172–6176. 10.1002/anie.200802376.

8. Jungmann, R., Avendaño, M.S., Woehrstein, J.B., Dai, M., Shih, W.M., and Yin, P. (2014). Multiplexed 3D cellular super-resolution imaging with DNA-PAINT and Exchange-PAINT. Nature Methods *11*, 313–318. 10.1038/nmeth.2835.

9. von Diezmann, A., Shechtman, Y., and Moerner, W.E. (2017). Three-Dimensional Localization of Single Molecules for Super-Resolution Imaging and Single-Particle Tracking. Chemical Reviews *117*, 7244–7275. 10.1021/acs.chemrev.6b00629.

10. Huang, B., Wang, W., Bates, M., and Zhuang, X. (2008). Three-Dimensional Super-Resolution Imaging by Stochastic Optical Reconstruction Microscopy. Science *319*, 810–813. 10.1126/science.1153529.

11. Enderlein, J., Gregor, I., and Ruckstuhl, T. (2011). Imaging properties of supercritical angle fluorescence optics. Optics Express *19*, 8011. 10.1364/OE.19.008011.

12. Bourg, N., Mayet, C., Dupuis, G., Barroca, T., Bon, P., Lécart, S., Fort, E., and Lévêque-Fort, S. (2015). Direct optical nanoscopy with axially localized detection. Nature Photonics *9*, 587–593. 10.1038/nphoton.2015.132.

13. Deschamps, J., Mund, M., and Ries, J. (2014). 3D superresolution microscopy by supercritical angle detection. 11.

14. Cabriel, C., Bourg, N., Jouchet, P., Dupuis, G., Leterrier, C., Baron, A., Badet-Denisot, M.-A., Vauzeilles, B., Fort, E., and Lévêque-Fort, S. (2019). Combining 3D single molecule localization strategies for reproducible bioimaging. Nat Commun *10*, 1–10. 10.1038/s41467-019-09901-8.

15. Bates, M., Keller-Findeisen, J., Przybylski, A., Hüper, A., Stephan, T., Ilgen, P., Delgado, A.R.C., D'Este, E., Jakobs, S., Sahl, S.J., et al. (2021). Optimal Precision and Accuracy in 4Pi-STORM using Dynamic Spline PSF Models (bioRxiv).

16. Huang, F., Sirinakis, G., Allgeyer, E.S., Schroeder, L.K., Duim, W.C., Kromann, E.B., Phan, T., Rivera-Molina, F.E., Myers, J.R., Irnov, I., et al. (2016). Ultra-High Resolution 3D Imaging of Whole Cells. Cell *166*, 1028–1040. 10.1016/j.cell.2016.06.016.

17. Bon, P., Linarès-Loyez, J., Feyeux, M., Alessandri, K., Lounis, B., Nassoy, P., and Cognet, L. (2018). Self-interference 3D super-resolution microscopy for deep tissue investigations. Nat Methods *15*, 449–454. 10.1038/s41592-018-0005-3.

18. Fort, E., Leveque-Fort, S., and Bourg, N. (2016). Systeme et procede de mesure d'un parametre physique d'un milieu.

19. Busoni, L., Dornier, A., Viovy, J.-L., Prost, J., and Cappello, G. (2005). Fast subnanometer particle localization by traveling-wave tracking. Journal of Applied Physics *98*, 064302. 10.1063/1.2043230.

20. Cappello, G., Pierobon, P., Symonds, C., Busoni, L., Christof, J., Gebhardt, M., Rief, M., and Prost, J. (2007). Myosin V stepping mechanism. Proc Natl Acad Sci U S A *104*, 15328–15333. 10.1073/pnas.0706653104.

21. Jouchet, P., Cabriel, C., Bourg, N., Bardou, M., Poüs, C., Fort, E., and Lévêque-Fort, S. (2021). Nanometric axial localization of single fluorescent molecules with modulated excitation. Nature Photonics, 1–8. 10.1038/s41566-020-00749-9.

22. Jouchet, P., Poüs, C., Fort, E., and Lévêque-Fort, S. (2022). Time-modulated excitation for enhanced single-molecule localization microscopy. Philosophical Transactions of the Royal Society A: Mathematical, Physical and Engineering Sciences *380*, 20200299. 10.1098/rsta.2020.0299.

23. Reymond, L., Reymond, L., Ziegler, J., Knapp, C., Wang, F.-C., Huser, T., Ruprecht, V., Ruprecht, V., and Wieser, S. (2019). SIMPLE: Structured illumination based point localization estimator with enhanced precision. Opt. Express, OE *27*, 24578–24590. 10.1364/OE.27.024578.

24. Cnossen, J., Hinsdale, T., Thorsen, R.Ø., Siemons, M., Schueder, F., Jungmann, R., Smith, C.S., Rieger, B., and Stallinga, S. (2020). Localization microscopy at doubled precision with patterned illumination. Nature Methods *17*, 59–63. 10.1038/s41592-019-0657-7.

25. Gu, L., Li, Y., Zhang, S., Xue, Y., Li, W., Li, D., Xu, T., and Ji, W. (2019). Molecular resolution imaging by repetitive optical selective exposure. Nat Methods, 1–5. 10.1038/s41592-019-0544-2.

26. Gu, L., Li, Y., Zhang, S., Zhou, M., Xue, Y., Li, W., Xu, T., and Ji, W. (2021). Molecular-scale axial localization by repetitive optical selective exposure. Nat Methods *18*, 369–373. 10.1038/s41592-021-01099-2.

27. Balzarotti, F., Eilers, Y., Gwosch, K.C., Gynnå, A.H., Westphal, V., Stefani, F.D., Elf, J., and Hell, S.W. (2017). Nanometer resolution imaging and tracking of fluorescent molecules with minimal photon fluxes. Science *355*, 606–612. 10.1126/science.aak9913.

28. Reymond, L., Huser, T., Ruprecht, V., and Wieser, S. (2020). Modulation-enhanced localization microscopy. Journal of Physics: Photonics *2*, 041001.

29. Schmidt, R., Weihs, T., Wurm, C.A., Jansen, I., Rehman, J., Sahl, S.J., and Hell, S.W. (2021). MINFLUX nanometer-scale 3D imaging and microsecond-range tracking on a common fluorescence microscope. Nat Commun *12*, 1478. 10.1038/s41467-021-21652-z.

30. Wolff, J.O., Scheiderer, L., Engelhardt, T., Engelhardt, J., Matthias, J., and Hell, S.W. (2023). MINFLUX dissects the unimpeded walking of kinesin-1. Science *379*, 1004–1010. 10.1126/science.ade2650.

31. Deguchi, T., Iwanski, M.K., Schentarra, E.-M., Heidebrecht, C., Schmidt, L., Heck, J., Weihs, T., Schnorrenberg, S., Hoess, P., Liu, S., et al. (2023). Direct observation of motor protein stepping in living cells using MINFLUX. Science *379*, 1010–1015. 10.1126/science.ade2676.

32. Gómez-García, P.A., Garbacik, E.T., Otterstrom, J.J., Garcia-Parajo, M.F., and Lakadamyali, M. (2018). Excitation-multiplexed multicolor superresolution imaging with fm-STORM and fm-DNA-PAINT. PNAS *115*, 12991–12996. 10.1073/pnas.1804725115.

33. Gustafsson, M.G.L. (2000). Surpassing the lateral resolution limit by a factor of two using structured illumination microscopy. Journal of Microscopy *198*, 82–87. 10.1046/j.1365-2818.2000.00710.x.

34. Fiolka, R., Shao, L., Rego, E.H., Davidson, M.W., and Gustafsson, M.G.L. (2012). Time-lapse two-color 3D imaging of live cells with doubled resolution using structured illumination. Proceedings of the National Academy of Sciences *109*, 5311–5315. 10.1073/pnas.1119262109.

35. Kner, P., Chhun, B.B., Griffis, E.R., Winoto, L., and Gustafsson, M.G.L. (2009). Super-resolution video microscopy of live cells by structured illumination. Nature Methods *6*, 339–342. 10.1038/nmeth.1324.

36. Schermelleh, L., Carlton, P.M., Haase, S., Shao, L., Winoto, L., Kner, P., Burke, B., Cardoso, M.C., Agard, D.A., Gustafsson, M.G.L., et al. (2008). Subdiffraction Multicolor Imaging of the Nuclear Periphery with 3D Structured Illumination Microscopy. Science *320*, 1332–1336. 10.1126/science.1156947.

37. Schermelleh, L., Heintzmann, R., and Leonhardt, H. (2010). A guide to super-resolution fluorescence microscopy. J Cell Biol *190*, 165–175. 10.1083/jcb.201002018.

38. Heintzmann, R., and Huser, T. (2017). Super-Resolution Structured Illumination Microscopy. Chem. Rev. *117*, 13890–13908. 10.1021/acs.chemrev.7b00218.

39. Li, M., Li, Y., Liu, W., Lal, A., Jiang, S., Jin, D., Yang, H., Wang, S., Zhanghao, K., and Xi, P. (2020). Structured illumination microscopy using digital micro-mirror device and coherent light source. Applied Physics Letters *116*, 233702. 10.1063/5.0008264.

40. Alice Sandmeyer, Mario Lachetta, Hauke Sandmeyer, Wolfgang Hübner, Thomas Huser, and Marcel Müller (2019). DMD-based super-resolution structured illumination microscopy visualizes live cell dynamics at high speed and low cost. Biorxiv.

41. Descloux, A., Müller, M., Navikas, V., Markwirth, A., Eynde, R. van den, Lukes, T., Hübner, W., Lasser, T., Radenovic, A., Dedecker, P., et al. (2020). High-speed multiplane structured illumination microscopy of living cells using an image-splitting prism. Nanophotonics *9*, 143–148. 10.1515/nanoph-2019-0346.

42. Lachetta, M., Wiebusch, G., Hübner, W., Esch, J.S. am, Huser, T., and Müller, M. (2021). Dual color DMD-SIM by temperature-controlled laser wavelength matching. Opt. Express, OE *29*, 39696–39708. 10.1364/OE.437822.

43. Chakrova, N., Canton, A.S., Danelon, C., Stallinga, S., and Rieger, B. (2016). Adaptive illumination reduces photobleaching in structured illumination microscopy. Biomed. Opt. Express, BOE *7*, 4263–4274. 10.1364/BOE.7.004263.

44. Brown, P.T., Kruithoff, R., Seedorf, G.J., and Shepherd, D.P. (2021). Multicolor structured illumination microscopy and quantitative control of polychromatic light with a digital micromirror device. Biomed. Opt. Express, BOE *12*, 3700–3716. 10.1364/BOE.422703.

45. Dupuis, G., Benabdallah, N., Chopinaud, A., Mayet, C., and Lévêque-Fort, S. (2013). Time-resolved wide-field optically sectioned fluorescence microscopy. In Three-Dimensional and Multidimensional Microscopy: Image Acquisition and Processing XX (SPIE), pp. 77–84. 10.1117/12.2003966.

46. Dan, D., Lei, M., Yao, B., Wang, W., Winterhalder, M., Zumbusch, A., Qi, Y., Xia, L., Yan, S., Yang, Y., et al. (2013). DMD-based LED-illumination Super-resolution and optical sectioning microscopy. Scientific Reports *3*. 10.1038/srep01116.

47. Lachetta, M., Sandmeyer, H., Sandmeyer, A., Esch, J.S. am, Huser, T., and Müller, M. (2021). Simulating digital micromirror devices for patterning coherent excitation light in structured illumination microscopy. Philosophical Transactions of the Royal Society A: Mathematical, Physical and Engineering Sciences *379*, 20200147. 10.1098/rsta.2020.0147.

48. Li, M., Li, Y., Liu, W., Lal, A., Jiang, S., Jin, D., Yang, H., Wang, S., Zhanghao, K., and Xi, P. (2020). Structured illumination microscopy using digital micro-mirror device and coherent light source. Applied Physics Letters *116*, 233702. 10.1063/5.0008264.

49. Sandmeyer, A., Lachetta, M., Sandmeyer, H., Hübner, W., Huser, T., and Müller, M. (2021). Cost-Effective Live Cell Structured Illumination Microscopy with Video-Rate Imaging. ACS Photonics *8*, 1639–1648. 10.1021/acsphotonics.0c01937.

50. Bossi, M., Fölling, J., Belov, V.N., Boyarskiy, V.P., Medda, R., Egner, A., Eggeling, C., Schönle, A., and Hell, S.W. (2008). Multicolor Far-Field Fluorescence Nanoscopy through Isolated Detection of Distinct Molecular Species. Nano Lett. *8*, 2463–2468. 10.1021/nl801471d.

51. Testa, I., Wurm, C.A., Medda, R., Rothermel, E., Middendorf, C. von, Fölling, J., Jakobs, S., Schönle, A., Hell, S.W., and Eggeling, C. (2010). Multicolor Fluorescence Nanoscopy in Fixed and Living Cells by Exciting Conventional Fluorophores with a Single Wavelength. Biophysical Journal *99*, 2686–2694. 10.1016/j.bpj.2010.08.012.

52. Lampe, A., Haucke, V., Sigrist, S.J., Heilemann, M., and Schmoranzer, J. (2012). Multi-colour direct STORM with red emitting carbocyanines. Biology of the Cell *104*, 229–237. 10.1111/boc.201100011.

53. Friedl, K., Mau, A., Boroni-Rueda, F., Caorsi, V., Bourg, N., Lévêque-Fort, S., and Leterrier, C. (2023). Assessing crosstalk in simultaneous multicolor single-molecule localization microscopy. Cell Reports Methods *3*, 100571. 10.1016/j.crmeth.2023.100571.

54. Gustafsson M.G., Shao L., Carlton P.M., Wang C.J., Golubovskaya I.N., Cande W.Z., Agard D.A., Sedat J.W. (2008). Three-dimensional resolution doubling in wide-field fluorescence microscopy by structured illumination. Biophysical Journal 94, 4957-70. 10.1529/biophysj.107.120345.